Bull. Spec. Astrophys. Obs., 1997, 43, 133–148

Photometry of OB stars on Hα images of M 33

S.N. Fabrika[a], O.N. Sholukhova[a], S.A. Zakharova[b]

[a] Special Astrophysical Observatory of the Russian AS, Nizhnij Arkhyz 357147, Russia
[b] Rostov State University, 344000 Rostov-on-Don, Bolshaya Sadovaya 105, Russia

Received December 24, 1996; accepted May 16, 1997.

Abstract. For the purposes of search for new SS 433 type objects, LBV stars and other similar unique stars in the galaxy M 33, we have carried out an identification and photometry of blue stars on Hα photographs of this galaxy. From 2332 known OB stars it was possible to do the photometry for 1619 stars. On the diagrams Hα flux — V magnitude we have isolated 549 emission-line objects, which have Hα excess among other stars of the same V magnitude. 81 Hα emitting stars have been selected from them on the diagrams Hα flux and Hα surface brightness — an object size. It has been found that about 334 selected candidates are extended objects having the properties of compact diffuse or bubble nebulae. A list of isolated objects, their morphological types, sizes and relative Hα fluxes are presented.

Key words: galaxy: photometry: individual (M 33): stars: OB — Hα excess

1. Introduction

This work has been done within the frames of the program of a search for new unique stellar objects in nearby galaxies, which we initiated in (Fabrika and Sholukhova, 1995). By unique or anomalously active objects we mean SS 433 — a massive binary system, where the supercritical accretion of a gas onto the relativistic star occurs, LBV (Luminous Blue Variables) — objects of S Dor and P Cyg types, Hubble–Sandage variables that show superpowerful outflow of winds in the atmospheres, and possible new types of like stars. All these objects are young single or binary stars, the brightest in the Galaxy. These stars in optical observations are similar to the object SS 433. In the Galaxy these stars are located in the disk, in the regions rich in gas and dust. Most of them are obscured from the observer because of considerable absorption of light. That is why we have launched the program of search for such objects in nearby galaxies. The most suitable for this purpose are nearby massive spiral nearly face-on galaxies, for instance, the galaxy M 33. It is important that this galaxy contains many young stars (Sharov, 1988) and is well studied. Ivanov et al. (1993) have compiled a catalogue of 2234 OB stars up to $V = 19^m.5$ in M 33. Assuming the number of hot and massive stars to be about 2000, Fabrika and Sholukhova (1995) have estimated the expected number of SS 433 type objects between 1 and 20.

Fabrika and Sholukhova (1995) have formulated basic criteria of a search for such objects in M 33. These criteria are mainly associated with similarity to SS 433. The object has to be 1) OB star and 2) Hα star, as SS 433 itself is a very powerful Hα source. Besides, the Hα line must be strongly variable. SS 433 Hα line equivalent width changes from 100 to 1000 Å (Vittone et al., 1983), while its FWHM is not less than 100 Å. Additional criteria are 3) He II λ 4686 emission, 4) the presence of a radio nebula around a candidate star, 5) a possible X-ray source, 6) brightness variability in the V-band up to 1^m on a time scale from days to years. Based on these criteria Fabrika and Sholukhova (1995) have made a preliminary analysis and selected 171 stars to be candidates for unique objects (the list 1). Criteria 1, 2 and 6 are common to SS 433 and LBVs, that is why it is worthwhile to make a concurrent search for such objects.

2. Preliminary selection of candidates

When making up the list 1 Fabrika and Sholukhova (1995) made cross-correlation analysis for coordinates of OB stars from Ivanov et al. (1993) and the star-like Hα sources from the list of Courtes et al. (1987). In the list 1 19 OB stars with $V \leq 18^m$ are presented, which are visible on the Hα images (Courtes et al., 1987) as stars brighter than the majority of OB stars of the same magnitude in V. The application of the Hα band used by Courtes et al. (1987) to a typical Hα line profile in the spectrum of SS 433 causes the object SS 433 in M 33 has to look on the Hα image by $\Delta m \gtrsim 1.4$ brighter than an OB star of the same magnitude in V. Proceeding from these estimates it has chosen the selection criterion $\Delta m \gtrsim 1^m$ by reason of a number of effects, which reduce reliability

of this procedure (see the discussion in Fabrika and Sholukhova (1995)). This selection was based on visual estimates, therefore the list 1 (Table 6 of Fabrika and Sholukhova (1995)) is rather incomplete. Besides it may contain only the brightest stars of $V < 18$. In this paper we examine OB stars on the Hα images on the basis of photometry of all objects from Ivanov et al. (1993). This catalogue comprises 2112 stars up to $V = 19^m.5$ which have been selected by the criteria $B - V < 0$, $U - B < 0$. It is not improbable that it includes star–like nebula too, as well as compact groups of stars. Here we use the 1st version of the catalogue (kindly made available by G. Ivanov prior to publication) containing 2234 objects with an addition of 98 objects taken from the catalogue published later (Ivanov et al., 1993). So we have studied on the Hα images a total of 2332 blue stellar objects.

3. Photometry of Hα images

We have used Hα photographs (contact copy from the original) obtained by Courtes et al. (1987) at the 6 m telescope with a focal reducer f/1. The Hα band had a width FWHM = 35 Å, the contribution of the nitrogen lines [N II] λ6548, 6584 is estimated as less than 10 %. The scale of the images is 34.5″/mm, the angular resolution is about 1″. All the images were digitized on the automatic microdensitometer (AMD) of SAO. A square diaphragm of 20 μm with a step of 20 μm (one pixel = 0.68″) was used for the recording. With an average image size of 1.5″ – 2″ such a recording does not affect the angular resolution.

At the initial stage we made a search for all blue stars on the Hα images of M 33, using their accurate coordinates. Even the finding chart taken from the B–band images (Ivanov et al., 1993) being available, it is far from being always possible to identify Hα object because of the dominant contribution of nebula and the strong Hα background. We used the coordinate grid (Fabrika, Sholukhova, 1995) from the plate measured with the Ascorecord, which had been obtained at the 1 m telescope of the Observatory of the Astronomical Institute of Tadjikistan AS (Sanglok). The accuracy of our measurements is 0.3″. As reference objects, 45 globular clusters were taken (Karimova, Sharov, 1981). When computing the coordinates, the program package created by V.V. Vlasyuk was used. From the stars and the objects, which are identified for certain, these coordinates were transferred to the Hα images. The accuracy achieved was about of 1″, which is better than that of the original catalogue (Ivanov et al., 1993) equal to 1.5″. All the catalogue stars were plotted on the Hα images with a three–fold error boxes. The objects that fell against a very strong Hα background were not considered. Photometry was done for 1619 out of 2332 stars. The probability of casual falling of the object within the error box with a side of 9″ is very low, it can be shown to be less than 2 % for 2000 stars in M 33. From our estimates the limiting stellar magnitude of a reliably measured OB star, which has no intrinsic Hα emission and is located in the outlying parts of the galaxy, is V = 18.5–19.0.

Photometry of the stars was performed with the program package developed by V.V. Vlasyuk. An object was measured with square diaphragms whose size was increased from 3 to 30 pixels with a step of 2 pixels (1.36″). The integral density in the diaphragm and the background density along the diaphragm's perimeter were measured. For the further study we used the density D, which is equal to the difference between the density inside the chosen diaphragm and the background D_b (average background per pixel multiplied by the diaphragm area). The object size (FWHM) was found in the next way. The level of half–intensity with subtracted background was found, and then the area at this level was put equal to an area of a circle with a diameter FWHM. Besides that, for the sake of inspection the size was also determined through a fitting of an object profile with the Gaussian in two orthogonal sections. Hereafter we will call the density as a flux, which is measured in our relative units, and denote it by F. As a rule, with a diaphragm size increasing both the integral flux and the object size grow, then these values get a plateau. The ordinate of the plateau is just a measured quantity. The dependence of the relative flux error $\sigma(F)/F$ on the flux shows that for faint objects the error does not exceed 10 %, for the main body of the objects it is less than 5 %. The size determination error is less than 30 % at FWHM $\approx$ 2″, less than 20 % at 3″ and below 5 % at sizes greater than 5″. We also tested a possible influence of an object position in the image (the edge effect) on the size measured accuracy. This could readily be done since the images were obtained (Courtes et al., 1987) with an overlap of 2′ – 3′. Analysis has shown that the change in the size of a star, as dependent on its position on the photograph, is well under the size measurement error. To diminish the personal error, any procedure described in this paper would has been performed by a single person.

Quite an essential point of our work is that we measured not the intensities but the densities. The measured flux (density) may be related to the intensity in a complicated fashion through two characteristic curves, original and copy. This fact does not have any effect on the selection of the stars having Hα line flux excess over the stars on the same image and of the same V magnitude, which is the principal result of the work. The relationship between the flux and intensity may be both linear, $F \propto I$ and logarithmic, $F \propto \lg I$, depending on which part of the effective characteristic curve we work. The former is the most likely case since we measure very faint objects, therefore it is

quite possible that we are working in the region of underexposures. Below we will be able to draw more definite conclusions.

4. Selection of candidates

In Fig.1 the relationship between flux F and magnitude V is presented for 148 stars of the eastern part of the galaxy M 33 (photograph No. 6, Courtes et al. (1987)). In this plot one sees distinctly the basic sequence of the stars without emission (filled circles) having no Hα excess and reflecting the fact that the stars that are brighter in the V band are brighter in the Hα band. In our case the flux in the Hα band will depend on magnitude V as $F = a\,10^{-(0.4V)}$ if the stars are on the lower ("nonlinear") part of the effective characteristic curve, and as $F = b - c\,0.4V$ or $F \propto \lg I$ if the stars are on the logarithmic ("linear") part of the curve. Approximations have shown that the first relation is valid. The exponential function satisfies the location of stars on the basic nonemission sequence much better than the linear. This means that we are working in the region of underexposures on the effective characteristic curve, where $F \propto I$. However, as we have already noted, the result of the selection of stars that have excess in Hα (open circles) does not depend on this dilemma.

The selection of candidates was performed in the following manner. In the intervals $\Delta V = 0.5$ the mean Hα flux value and its standard deviation were found, the stars, whose flux deviation from the mean was over 2σ, were rejected. Then approximation of the curve from the remaining objects was done, the stars with a deviation greater than 2σ were rejected and this process was repeated. The described procedure converges after 2–3 iterations. The "cleaned" basic sequence of the nonemission stars and its deviation σ were thus obtained. Then the stars were isolated whose flux departed from it upwards by a value greater than 2σ. This selection criterion (2σ) is a "soft" enough, and it has been chosen in order to not miss possible interesting stars with a weak Hα emission. The selected stars are the objects sought with a flux excess in the Hα over OB stars without emission by a value higher than 2σ of the basic sequence scatter. All in all 549 objects were selected.

On the basis of our photometry data we may estimate the Hα line equivalent width. One may find that the quantity $W'_\lambda = \Delta\lambda \cdot ((F - F_{ms})/F_{ms})$ is the line equivalent width estimate, where $\Delta\lambda$ is the FWHM of the Hα band, F_{ms} is the flux on the basic star sequence in the given interval of magnitudes. It is very important to note, that it is proposed in definition of the W'_λ, that the emission line is radiated both in a whole nebula and in a star's atmosphere, but the continuous spectrum is stellar. In such a case this value W'_λ is a direct function of the star UV luminosity beyond the Lyman edge over that in the V band, i. e it is a function of the star temperature. The W'_λ determination error is:

$$\sigma(W_\lambda) = (W_\lambda + \Delta\lambda)\frac{\sigma(F)}{F}\left(1 + \left(\frac{F}{\sigma(F)} \cdot \frac{\sigma_{ms}}{F_{ms}}\right)^2\right)^{1/2},$$

where σ_{ms} is the error of the mean flux value in the basic sequence, $\sigma(F)/F$ is the relative error of the flux measurement. In Fig. 2 the relation between the relative equivalent width error $\sigma(W'_\lambda)/W'_\lambda$ and W'_λ is presented. The solid lines show the family of curves for minimal fluxes $F < 1000$, the dashed lines are for maximal fluxes $F > 5000$, the numbers at the curves indicate the intervals of stellar magnitudes: 1 corresponds to V = 15.5–17.5, 2 to 17.5–18.5, 3 to 18.5–19.5. The division was done for convenience since the value of σ_{ms}/F_{ms} depends on stellar magnitude (see Fig. 1). It is seen that even for the faintest stars the error is on the average not larger than 40 % at $W'_\lambda > 20$ Å. In more details the sense of the value W'_λ obtained by the described procedure will be discussed below.

The objects we have selected, which have emission in Hα are listed in Table 1, where the columns present: 1) the successive numbers, 2) the stellar magnitudes V, 3) $S = (F - F_{ms})/\sigma$ — the flux excess over the flux of the basic (nonemission) star sequence, which is measured in standard deviations of the stars composing this sequence, 4) the Hα equivalenth width estimate W'_λ in angstroms, 5) the size of objects in arcseconds, 6) an object type (the explanation for the last column will be given below) and 7) the number from the original catalogue (Ivanov et al., 1993). For the last 35 objects the numbers are taken from the first unpublished version of the catalogue because they were excluded in the paper by Ivanov et al. (1993).

5. The flux–size relationship

The early stars with Hα emission we have isolated may have either intrinsic emission (the objects of our search), or be stars in H II regions. Possibly these are Hα nebulae in which the visibility of the central ionizing star in the V band depends on the contribution of the nebula lines to this band. After spectroscopy of the selected objects it will be possible to definitely answer the question, however, examination of Fig. 3 can considerably clear up the situation. On the plot Hα flux — size for all measured objects of the image No. 6 from Courtes et al. (1987) (little circles) the objects are readily seen to be divided into two (or possibly three) branches. It is natural to connect this division with different morphological types of the objects: the lower sequence represents stars, the upper (or two upper sequences) — nebulae or stars plus

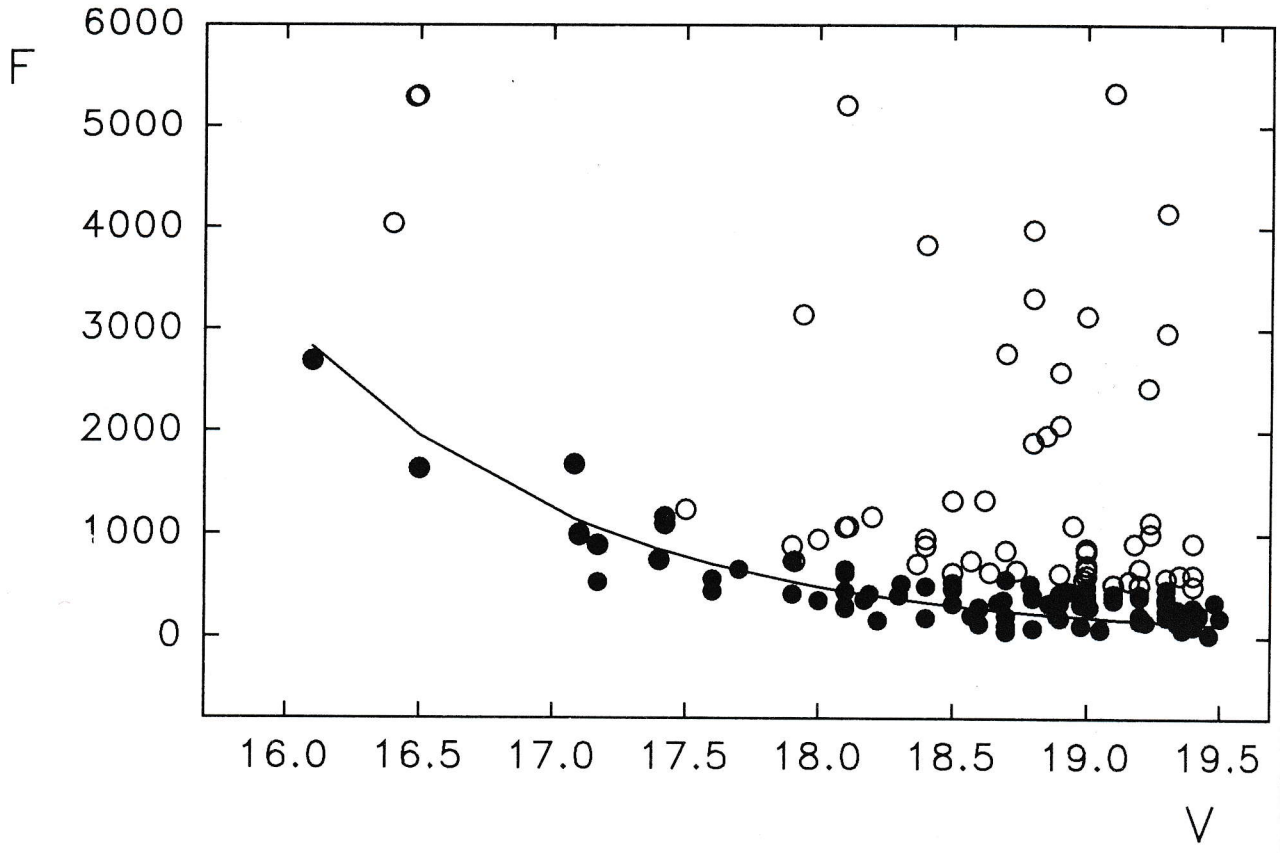

Figure 1: *Hα line flux F vs V magnitude for 148 measured stars of the image No. 6 of the eastern part of M 33. The stars selected by the criterion of flux excess are shown by the open circles, the stars that comprise the basic sequence of nonemission stars — by the filled circles.*

nebulae. On the image there appeared to be about 60 % extended objects, 20 % of stellar objects and also about 20 % of the objects located in the lower–left corner of the diagram of Fig. 3 at the place of a junction of all branches.

It is known that a compact H II region can imitate a hot star in the U–B, B–V colours and may also be a star–like source (in M 33 $1'' = 3.5$ pc). Nebulae (or nebulae with a visible star) may well be included in the catalogue of hot stars (Ivanov et al., 1993). For star–like objects the flux must be $F \propto 10^{\alpha d}$, where d is the size of a star on a plate (Zickgraf, Humphreys, 1991). In the case of a supernova remnant or a bubble–type nebula $F \propto d^2$, in the case of a filled or a diffuse nebula $F \propto d^3$, an intermediate power sequence is also possible depending on the morphology of a nebula and a star contribution in the Hα band.

The results of testing this interpretation are contained in Fig. 3. There from the same image we plot a number of objects, whose morphology is obvious: apparent but not very bright stars (triangles), large bubble–type nebulae (squares), "core plus halo"–type nebulae and diffuse nebulae (circles). The small circles indicate the objects from Fig. 1. It is seen from Fig. 3 that stars fall on lower star sequence, bubbles on the uppermost sequence, to be more precize, on its continuation. The third, intermediate sequence is continued by diffuse and "core plus halo" nebulae. All three sequences join naturally in the region of objects' sizes $1'' - 2.5''$.

The apparent separation of the objects in Fig. 3 provides grounds to break up all the studied objects on the basis of their morphological features in Hα into sequences: stars, bubble nebulae and intermediate diffuse (or complex) nebulae. The objects having low fluxes and small sizes are common to all three sequences. We label these 4 groups by s, d, b and c, respectively. It should be emphasized that the division can be done only on the average. Some of the objects fill space between the sequences, which is caused not only by photometric errors but by the real complex morphology of the nebulae.

We made approximations of each of the isolated sequences (Fig. 3) with the inclusion of the objects of known types (bold lines) and only for the objects of the catalogue (Ivanov et al., 1993) (thin lines). The objects of type c were added, when approximating,

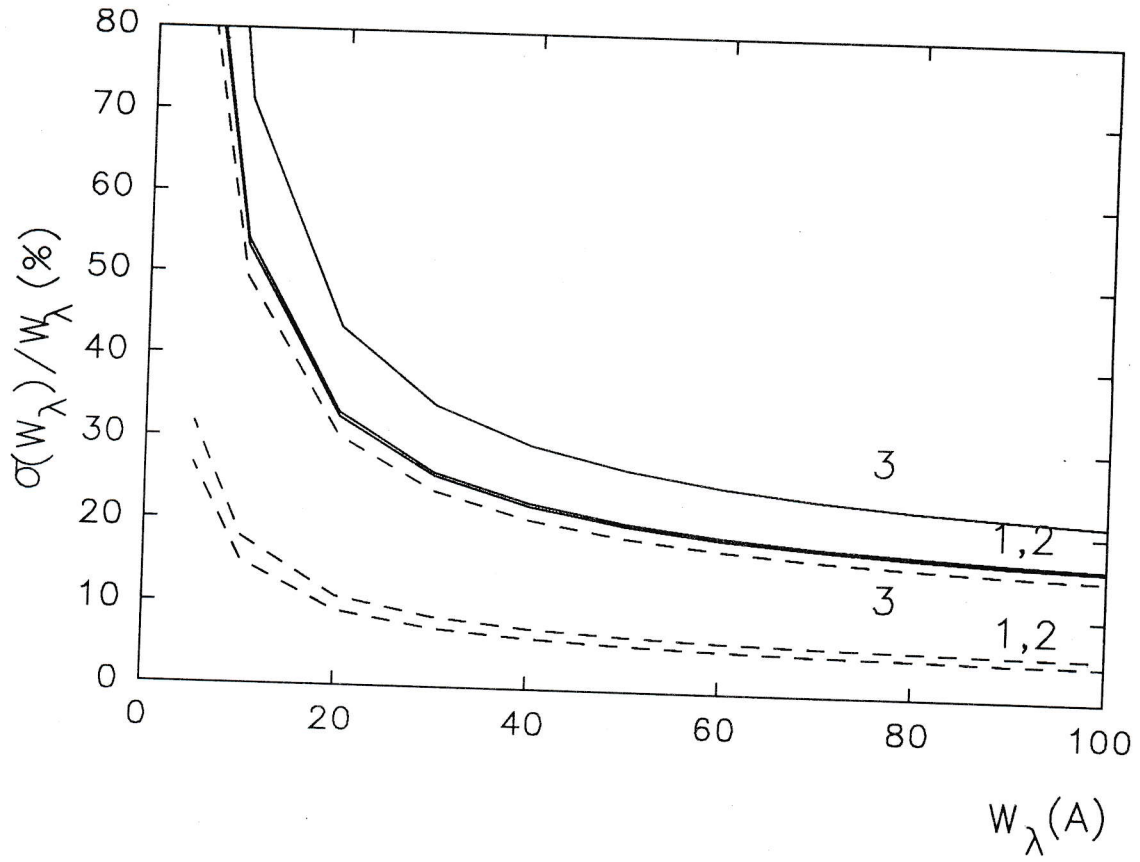

Figure 2: *The errors of the Hα equivalent width estimates* W'_λ. *The curves for the objects with minimal Hα fluxes,* $F < 1000$, *are solid lines, those for maximal fluxes,* $F > 5000$, *are dashed lines. The numbers at the curves show the intervals of stellar magnitudes: 1 — V = 15.5–17.5; 2 — 17.5–18.5; 3 — 18.5–19.5.*

to all three sequences. For both versions of the stellar sequence $F = F_0 \cdot 10^{ad} + b$ turned out optimum. By equalling the flux to zero, we find an estimate of the seeing size d_0 in a given image. In particular, in Fig. 3 d_0 equals 1.8″ and 1.6″ both for all stars and only for the catalogue stars, respectively.

The bubble sequence must satisfy $F \propto d^2$. A formal search for the best curve describing this data by the power function $F \propto d^n$ yields $n = 1.95$–2.05, i.e. the square power does fit this type of objects. Approximations of these two samples (with the inclusion of the known bubbles and without them) by $F = F_0 \cdot d^2 + a$ yields a good fitness, the seeing estimate is 1.7″.

In Fig. 3 are also presented the approximations of the intermediate type (diffuse) nebulae. One may propose that the appearance of the diffuse sequence may be due to inaccuracies in determining the parameters of the objects of complex structure. However, the fact that the bright diffuse nebulae fit well the intermediate sequence is a forcible argument in favour of reality of the intermediate objects as a separate diffuse sequence. Approximation of this sequence by $F \propto d^n$ yields $n = 3.2 \pm 0.3$, i. e. the cubic power describes well the diffuse branch (the seeing estimate $d_0 = 2.0''$).

It should be noted that the approximation results in themselves prove that we are working on a nonlinear part of the effective characteristic curve. When examining the rest of the images of M 33 from Courtes et al. (1987), we applied quite similar techniques. The images of the central region of the galaxy, however, are characterized by a stronger background and their position on the effective characteristic curve is likely to be shifted forwards the linear region, where $F \propto \lg I$. The conclusions drawn from a single Hα image were confirmed for the remaining 8. The seeing estimate for all the photographs is $1.8'' \pm 0.1''$, what is in agreement with the real seeing value during the observations (Courtes et al., 1987).

A relationship between a size d and surface brightness $SB = F/d^2$ has been studied for the selected candidates. Such a plot for one of the central images is presented in Fig. 4. As it was to be expected the objects broke up into three sequences according to these described above. In this representation, some of the objects of type c is easier to identify and refer them to one of the sequences s, d or b. We made the approximations in Fig. 4 (dotted lines) using both the objects broken up into sequences s, d, b and the c–

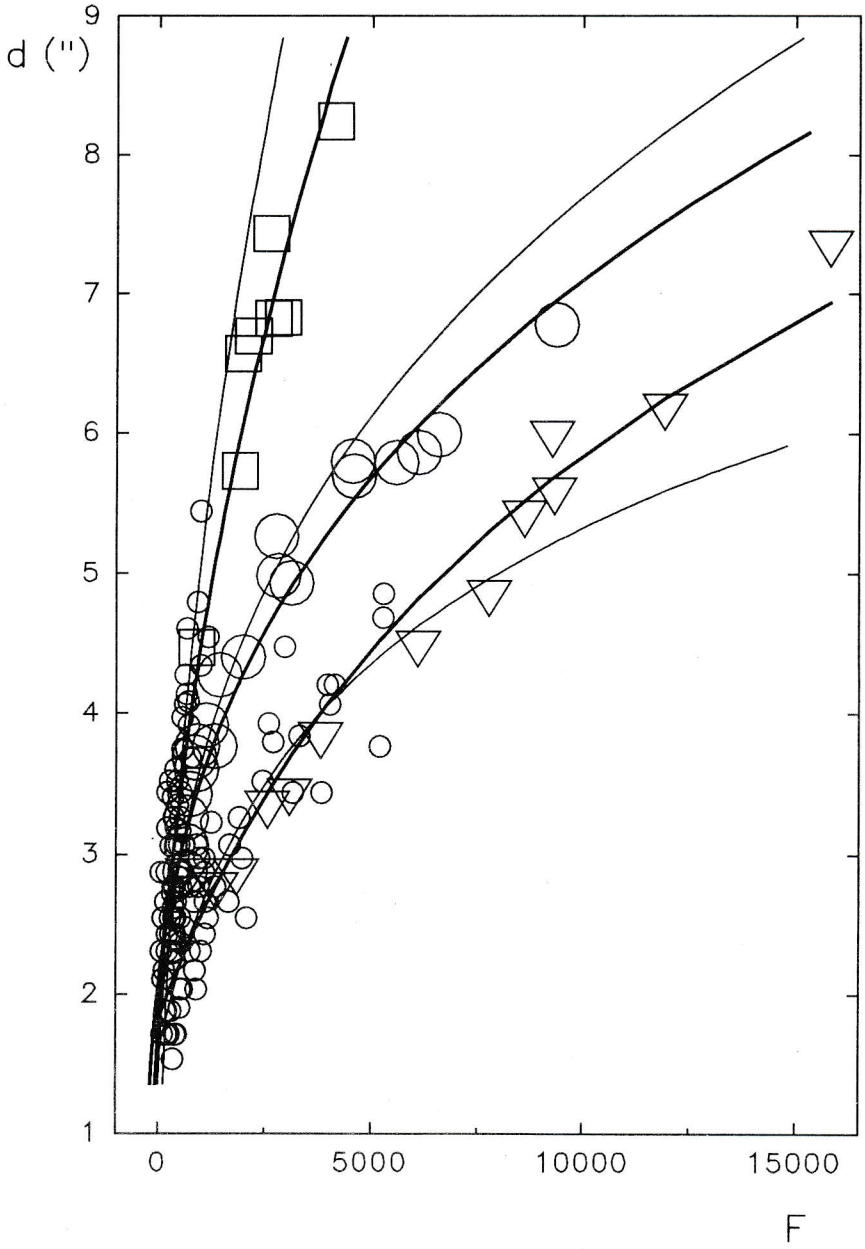

Figure 3: *An object size (FWHM) as a function of flux F in the Hα band for the same stars as in Fig. 1. Division into star and nebula sequences is seen. Apart from the objects studied there also shown brighter stars (triangles) and obvious nebulae — bubbles (squares) and diffuse (large circles) from the same image. The bold lines show the approximations of the sequences with bright stars and nebulae included, the thin lines are those for the objects of the catalogue (Ivanov et al., 1993) only.*

type objects close to the each sequence in the form:

$$SB = \begin{cases} (a + c10^{\alpha d})/d^2 \\ (a + cd^3)/d^2 \\ (a + cd^2)/d^2, \end{cases}$$

where the coefficients a, c and α were determined for each sequence and in each image separately.

Despite the fact that the curves, on the average, describe fairly the sequences, especially the star sequence (the upper curve in Fig. 4), it is quite possible to improve the fits. For this purpose the photographic effect of a star size growing with star brightness has to be taken into account. For the extended objects this is most essential with small size of nebulae. From the analysis of Fig. 4 it can be concluded that with nebulae sizes of $2'' - 4''$ the curves (two lower dotted lines) overestimate the value of SB, i. e. the data themselves are located, on the average, below the curves. To allow for this effect, it has to be added to the formula of the nebulae flux ($F(d) = A + F_0 d^n$)

a term, which describes the behaviour of a point–like source, $F(d) = (A + B\,d^{2n} + C \cdot 10^{\beta d})^{1/2}$. Taking $F_0\,d^n$ out of brackets and expanding the rest into a series with $d = d_0$, one can find that the allowance for the photographic effect can be made by adding to the flux expression a linear term $F(d) = A + F_0\,d^n + kd$. The solid lines in Fig. 4 show the b and d–type object approximations with the linear term allowed for. Agreement between the curves and the data for the nebulae is seen to considerably improve. With the aid of the diagram SB—d we managed to isolate a part of the objects from the group c and refer them to one of the three morphological sequences.

6. Discussion

Thus, all the isolated objects with Hα excess were divided into sequences on the basis of morphological features of their Hα images: stellar (s), diffuse nebulae sequence (d), bubble–type nebulae (b), the objects that remained unclassified were labeled by c. These designations are presented in the last column of Table 1. Besides, there were objects for which it turned out to be impossible to determine the size because of their closeness to bright H II regions. As a rule, on the Hα image these objects are seen as a hump near a large nebula, i. e. they are located on a steep background gradient. In the methods of a size measurement we used, their size would often be underestimated or equal to zero. 17 such objects in Table 1 are denoted as zs. As a result of break up of the selected objects into sequences there were isolated 81 stars, 154 diffuse nebulae, 180 bubbles, and 117 objects of type c.

From the examination of Table 1 it follows that the objects having a maximal excess in the Hα band belong mostly to the diffuse nebulae sequence, while the objects with a minimal excess to the sequence of bubbles. In the next paper by Fabrika and Sholukhova (1997) a more detailed analysis of these objects is presented. It is necessary to discuss here how the value W'_λ we have obtained is related to the Hα line equivalent width W_λ. W'_λ depends on the H II region size that surrounds the star, which in turn is determined by the star's temperature and luminosity, electron density and other parameters of the medium. The sizes d and the Hα line fluxes measured (quantities F, S or W'_λ) may be of independent interest for finding the isolated nebulae and their central stars parameters. However, if we want to estimate the line equivalent width as the emission line flux from the star in units of the star continuous radiation flux, we have to reduce the flux value F as if it be measured in an aperture $\approx 1''$, — $W_\lambda \approx W'_\lambda/d^2$, where d is the nebula size in arcseconds. Such a correction reduces the derived fluxes to a standard spectroscopic aperture. Even after that the line equivalent width estimates may be in error. The equivalent widths we have obtained will be accurate only for stars with intrinsic Hα emission. The selection of such stars (for instance, by the criterion of Hα line broadening) as well as the final identification of the isolated object is possible only after spectroscopy.

Calzetti et al. (1995) have recently published the results of a systematic search for SS 433–type candidates in the galaxy M 33. To isolate candidates they used CCD images of M 33 in a narrow Hα band and in an adjacent continuum at about 6100 Å. They have estimated the limiting stellar magnitude $V \approx 20$. The M 33 field coverage by the Calzetti et al. (1995) images is approximately twice as small as the region we have studied. Their fields contain 311 from 549 objects we have selected. Calzetti et al. (1995) have isolated a total of 279 compact H II regions and 153 point–like emission sources (actually they have found a somewhat smaller number of objects since analysis of the Hα images reveals that their samples contain 27 object repetitions). Comparing our Table 1 with the data of Calzetti et al. (1995), we found 42 common objects, 17 of them among H II regions and 25 from the list of point–like emission objects. The greater part of these H II regions belong to our sequence of diffuse nebulae. A half of these point-like Hα sources are also among diffuse nebulae, while the rest of the objects are of types s and c. The list of Calzetti et al. (1995) comprises 64 % of H II regions and 36 % of star–like objects. Our sample (Table 1) contains 63 % of d– and b–type nebulae, 15 % of s–type and 22 % of c–type objects, i. e. 37 % of star–like emission objects. The relative proportions of extended and star–like objects in this paper and in Calzetti et al. (1995) are in excellent agreement with each other. The incomplete overlapping of the two samples is likely due to the fact that Calzetti et al. (1995) have examined only the central regions of M 33, where the great Hα background inhibits the separation of emission objects in the photographic data we used. For this reason the two lists may be considered as complementing each other.

7. Conclusion

In this paper identification and photometry of OB stars on Hα images of the galaxy M 33 have been performed. Out of 2332 blue stars of the Ivanov et al. (1993) catalogue we have managed to identify and measure 1619 objects in Hα. On the Hα flux — V magnitude diagrams the star without noticeable emission form a nonemission sequence above which emission–line objects are located. Their Hα emission may be both the intrinsic radiation of the star's envelope and the radiation of a compact H II region around the star. All in all 549 objects have been isolated by the criteria of the Hα excess. Based on the

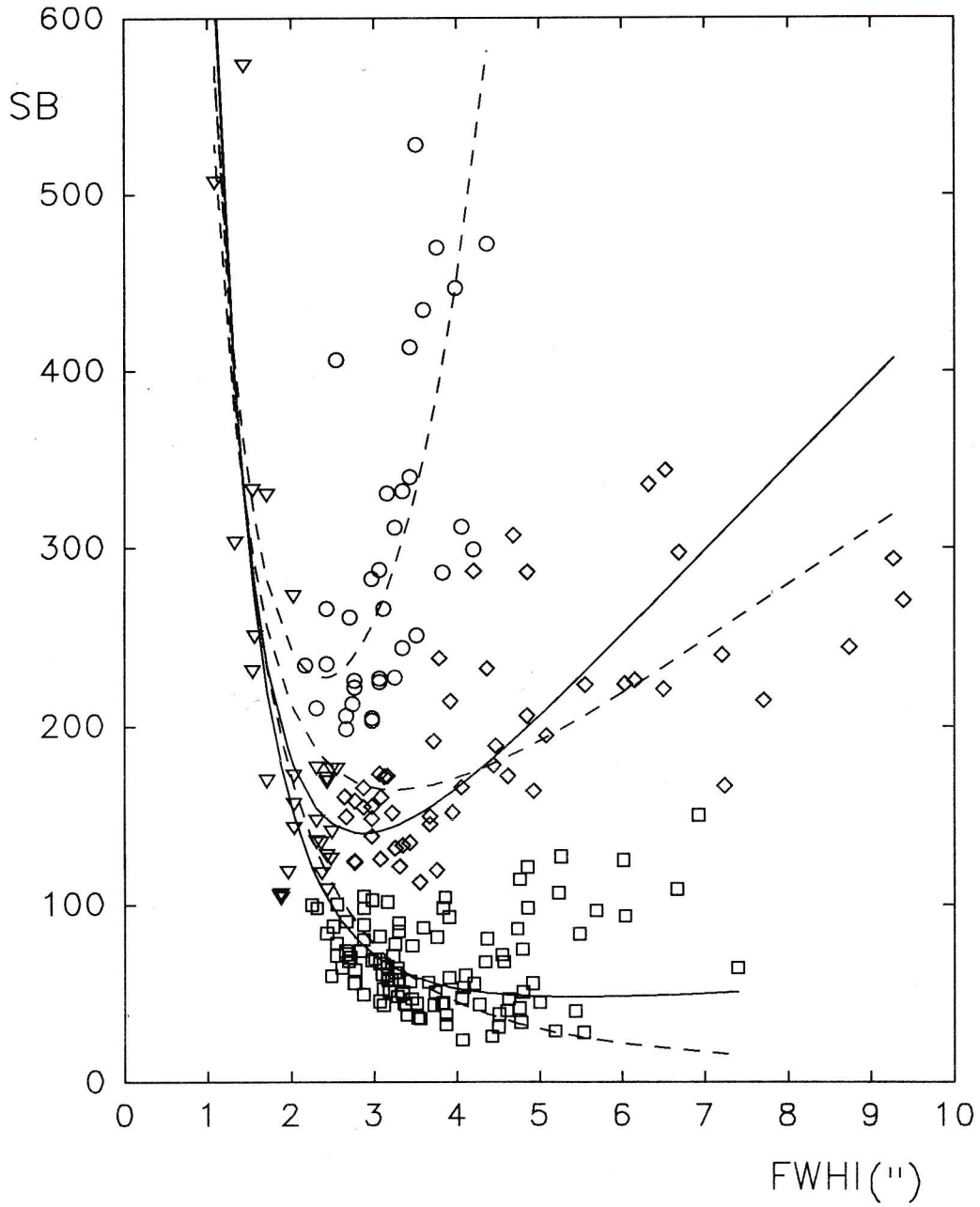

Figure 4: *Relationship between the Hα surface brightness and the object sizes for the image No. 2 from Courtes et al. (1987). Stars — circles, diffuse nebulae — diamonds, bubbles — squares, common point-like objects — triangles. The approximations of the isolated sequences (dashed lines) and those with allowance for the photographic effect for the extended objects (solid lines).*

relationships Hα line flux — an object size and a size — surface brightness, it has been found that 334 or 60 % of the candidate stars are extended objects having the characteristics of diffuse nebulae or bubbles. There have also been isolated 81 stars and 117 compact star–like emission sources.

Acknowledgements. We wish to thank V. V. Vlasyuk for providing us with program package for processing the images, G. R. Ivanov for use of his catalogue prior to publication, S. N. Dodonov for Hα photographs made available, to N. A. Tikhonov and T. B. Georgiev for helpful discussions. The work was supported by grant No.3–13 of the

Program "Astronomy" RAS and ESO grant No. A–02–021 of the C&EE Program. O.N. Sholukhova is grateful to the American Astronomical Society for support by a grant. S.N. Fabrika was supported by a grant of ISF.

References

Calzetti D., Kinney A.L., Ford H., Doggett J., Long K.S, 1995, Astron. J., **110**, 2739

Courtes G., Petit H., Sivan J.-P., Dodonov S., Petit M., 1987, Astron. Astrophys., **174**, 28

Fabrika S.N., Sholukhova O.N., 1995, Astrophys. Space Sci., **226**, 229

Fabrika S.N., Sholukhova O.N., 1997, Bull. Spec. Astrophys. Obs., **43**, (this issue), 149

Ivanov G.R., Freedman W.L., Madore B.F., 1993, Astrophys. J. Suppl. Ser., **89**, 85

Karimova D.K., Sharov A.S., 1981, Pis'ma Astron. Zh., **7**, 265

Sharov A.S., 1988, Spiral galaxy M 33, Moscow, Nauka, 248

Vittone A., Rusconi L., Sedmak G., Mammano A., Ciatti F., 1983, Astron. Astrophys. Suppl. Ser., **53**, 109

Zickgraf F.-J., Humphreys R.M., 1991, Astron. J., **102**, 113

Table 1. Selected emission objects

n	m_V	S	W_λ (Å)	d^1 ($''$)	Type	N^2 [3]	n	m_V	S	W_λ (Å)	d^1 ($''$)	Type	N^2 [3]
(1)	(2)	(3)	(4)	(5)	(6)	(7)	(1)	(2)	(3)	(4)	(5)	(6)	(7)
1	18.80	3.7	47	3.0	b	8	41	17.00	10.6	36		s	208
2	18.50	6.6	63		c	11	42	18.47	6.0	77	4.0	d	210
3	18.40	5.7	50	2.8	d	18	43	17.97	4.6	28	3.2	b	211
4	18.60	2.9	32	3.2	b	22	44	18.60	13.4	129	3.1	d	215
5	18.70	51.9	372		s	42	45	18.81	41.6	346	6.0	b	216
6	19.10	33.9	359	4.6	d	60	46	17.70	5.9	28	3.0	d	222
7	19.20	68.3	532	6.9	b	61	47	18.90	2.5	36	3.9	b	227
8	16.67	7.5	14		s	65	48	18.35	5.8	49	4.2	b	228
9	19.30	10.0	173	5.4	b	68	49	17.20	32.4	90	4.4	d	240
10	19.00	5.2	78	3.2	b	71	50	18.70	2.1	34	5.5	b	246
11	18.65	23.0	207	3.7	d	72	51	18.39	2.6	24		c	248
12	18.00	6.4	40	3.1	d	87	52	17.81	13.5	68	3.7	d	263
13	18.31	3.2	26		c	90	53	17.30	42.2	186	6.7	d	268
14	18.58	3.2	34	2.7	b	99	54	18.10	4.8	33	3.3	b	272
15	18.24	6.5	50		c	101	55	16.80	7.4	16	3.9	d	276
16	18.70	3.2	38		c	104	56	19.10	8.7	202		c	282
17	18.80	14.3	160		s	109	57	19.19	7.1	119	3.0	b	284
18	18.20	16.2	111		s	116	58	19.42	6.0	185		c	285
19	18.60	12.9	125	3.1	d	119	59	18.60	24.0	350		s	298
20	18.70	5.8	66		c	120	60	16.40	4.0	6	4.1	d	301
21	19.22	12.5	194		s	125	61	18.80	1.9	26		c	329
22	17.80	60.7	239	5.6	d	131	62	19.10	2.0	47		c	337
23	19.50	11.6	224	3.3	d	136	63	19.40	6.2	126		c	341
24	17.79	389.9	620		zs	137	64	17.83	6.5	211	5.7	b	343
25	17.70	10.8	50		s	139	65	18.90	12.4	237	3.8	d	344
26	18.70	3.6	42	3.8	b	140	66	19.02	3.0	46	2.7	b	350
27	18.80	8.4	101	2.6	d	141	67	19.30	82.8	4713	9.0	d	352
28	18.40	5.8	51		c	143	68	19.00	18.6	83		s	361
29	18.40	1.9	18	3.5	b	147	69	18.40	2.9	34	4.0	b	366
30	19.48	2.8	65	3.1	b	156	70	17.80	15.9	110		s	368
31	18.91	5.4	74	4.5	b	162	71	19.38	17.7	279	3.7	d	369
32	18.40	13.2	108	4.8	b	168	72	19.10	7.8	442		s	372
33	17.71	5.6	27	2.9	d	169	73	17.12	11.0	372		s	374
34	19.00	2.1	33	2.8	b	172	74	18.33	11.2	88	4.4	b	382
35	18.79	6.7	82	4.8	b	174	75	19.19	4.6	114		c	383
36	17.70	2.9	14		c	188	76	17.30	8.3	36		s	386
37	17.61	10.0	43		s	192	77	19.30	7.3	203		c	392
38	19.48	3.8	124	4.9	b	200	78	17.70	2.6	33	3.0	d	401
39	19.27	81.7	581	6.2	d	202	79	19.47	40.0	2665	5.3	d	403
40	19.49	2.5	60	4.1	b	205	80	16.90	14.1	43		s	404

Table 1 (continued)

(1)	(2)	(3)	(4)	(5)	(6)	(7)	(1)	(2)	(3)	(4)	(5)	(6)	(7)
81	19.36	5.6	164	3.9	b	406	121	16.80	15.3	42		s	548
82	19.10	9.3	140		c	408	122	19.20	84.0	2129		s	550
83	18.68	25.6	230	5.2	b	409	123	18.80	2.2	38	3.3	b	555
84	18.00	10.3	62	3.4	d	411	124	17.72	5.3	34		s	559
85	18.60	29.2	871	5.1	d	412	125	17.69	5.0	32		s	561
86	19.21	3.3	60	3.1	b	417	126	17.58	19.9	232		s	571
87	19.42	4.5	97		c	420	127	19.16	6.1	148		c	574
88	19.01	24.5	277		s	422	128	19.10	9.2	212	4.4	d	578
89	19.00	68.3	1440	7.1	d	424	129	18.97	3.1	63	3.1	b	584
90	19.34	8.9	256	4.2	d	425	130	18.22	20.0	421	5.8	d	589
91	17.20	5.9	18	3.2	d	426	131	18.60	24.8	361	5.1	d	592
92	17.99	2.3	19		c	431	132	19.42	4.7	296		c	607
93	19.21	3.2	166		c	432	133	18.66	5.6	62	5.5	b	609
94	17.60	6.8	61	3.5	d	435	134	17.00	8.9	29	5.3	d	611
95	18.50	2.1	28	3.3	b	442	135	17.20	9.3	482		s	614
96	17.28	9.8	557		s	444	136	17.40	9.3	45	4.1	d	619
97	18.78	4.9	61	4.8	b	449	137	19.40	36.5	1112	7.3	d	629
98	19.17	4.1	102	4.3	b	452	138	18.70	6.7	384	3.6	d	630
99	18.90	2.8	53	5.3	b	454	139	19.30	117.6	6692	10.5	d	633
100	18.39	30.9	217	7.4	b	455	140	18.75	4.4	74	3.6	b	637
101	18.68	2.1	25	3.4	b	465	141	18.40	13.7	166	4.9	d	639
102	19.33	22.9	322	5.5	b	466	142	17.90	4.2	24	4.1	b	644
103	18.40	2.8	33		c	467	143	19.11	7.3	212	3.5	d	646
104	19.10	169.8	3926		zs	471	144	18.10	2.7	25	3.5	b	648
105	18.96	28.3	296	5.7	b	482	145	19.17	3.9	68	3.2	b	651
106	19.20	60.9	93	6.5	d	488	146	18.90	11.7	225		s	653
107	18.22	2.2	23		c	490	147	19.42	7.5	231		c	656
108	18.95	5.4	77	5.2	b	492	148	19.46	2.8	65	3.1	b	663
109	19.40	18.6	1157	7.7	b	493	149	18.50	20.3	380	5.9	d	664
110	18.10	2.7	50	3.2	b	500	150	19.34	30.0	864		s	666
111	18.15	3.1	30		c	505	151	19.00	4.1	62	4.5	b	667
112	18.70	13.2	211	4.5	d	511	152	17.70	4.2	27		c	669
113	16.50	2.1	9	4.0	d	515	153	19.40	11.4	348		s	675
114	18.70	4.9	78	3.6	b	526	154	18.50	2.6	71		c	676
115	18.62	2.6	78		c	527	155	19.50	4.4	147		c	677
116	18.85	14.0	525	7.7	b	532	156	18.70	42.2	675	9.3	b	678
117	18.60	252.6	3686		zs	533	157	19.20	2.8	71		c	689
118	19.43	2.4	74		c	536	158	18.17	2.7	26	3.8	b	697
119	18.60	7.7	71	4.3	b	537	159	18.00	17.4	100	4.9	b	699
120	17.90	8.2	62	4.2	d	544	160	16.99	34.0	79	4.9	d	701

Table 1 (continued)

(1)	(2)	(3)	(4)	(5)	(6)	(7)	(1)	(2)	(3)	(4)	(5)	(6)	(7)
161	19.00	19.8	417	4.5	d	705	201	19.00	7.8	232	4.1	d	821
162	19.00	10.7	225	4.9	d	710	202	18.80	10.7	124	4.9	b	823
163	17.68	62.7	803	7.2	d	712	203	18.10	6.4	192	4.3	b	825
164	18.84	3.7	40	3.4	d	714	204	19.10	5.1	169		zs	830
165	18.40	8.5	103	3.9	d	718	205	19.00	6.9	145	4.4	b	836
166	16.90	9.8	30	4.8	d	719	206	18.90	8.2	293		zs	837
167	16.80	16.2	45		s	727	207	16.70	3.6	18		zs	839
168	18.70	13.5	215	4.9	d	730	208	18.80	13.1	76		zs	842
169	18.40	6.0	72		c	734	209	19.20	3.6	91		c	844
170	19.00	61.3	93	7.9	d	735	210	19.30	9.7	269	4.5	d	853
171	16.40	15.5	30	5.9	d	736	211	17.90	8.8	49	3.3	d	856
172	18.80	6.9	120	4.2	b	740	212	18.90	53.0	2086	8.5	d	861
173	15.87	3.2	4		s	743	213	18.60	4.0	119	2.9	d	863
174	19.36	60.0	3608	8.7	d	747	214	18.84	3.9	145		c	867
175	19.30	7.6	58		zs	749	215	18.30	12.0	132	4.4	d	868
176	16.77	6.7	35		s	750	216	19.00	36.3	766	8.9	b	870
177	19.40	7.3	221		c	751	217	18.66	8.9	137	4.3	d	874
178	17.84	3.0	16	3.5	b	755	218	18.90	8.7	113	5.0	b	875
179	17.20	9.7	39	4.8	d	757	219	18.10	5.7	139		s	878
180	18.70	2.0	66		c	760	220	18.60	2.4	26	3.5	b	879
181	18.20	2.2	22		c	761	221	18.22	16.8	173	4.7	d	884
182	18.10	2.8	53		c	771	222	18.48	3.1	40		c	895
183	19.01	38.1	1659	6.4	d	772	223	18.60	6.6	237	4.4	b	905
184	18.90	8.5	105	4.6	b	774	224	19.30	14.9	846	5.3	d	910
185	19.10	2.4	114		c	775	225	19.20	2.7	68	3.4	b	913
186	18.20	6.0	60		c	779	226	17.50	11.9	128	5.0	d	920
187	18.60	6.3	91	5.0	b	780	227	18.40	9.7	117	4.0	d	923
188	18.91	4.0	78	3.5	b	781	228	18.30	241.3	617	9.3	d	926
189	19.40	2.1	64		c	783	229	19.20	6.2	61		zs	933
190	18.80	3.3	42	3.2	b	784	230	19.20	15.6	395		s	935
191	18.30	6.3	70		c	786	231	19.10	2.9	136		c	936
192	19.20	27.5	1429	6.2	d	789	232	17.50	7.0	37	4.0	d	938
193	18.85	2.1	39		c	790	233	18.38	6.0	223		s	948
194	18.80	5.2	205		zs	791	234	19.40	3.7	113		c	953
195	18.50	3.3	90		c	795	235	17.90	10.6	289		s	956
196	19.00	57.8	2493	7.6	d	799	236	19.31	2.4	136		c	965
197	19.13	2.3	113		c	803	237	18.30	6.1	116	4.2	b	976
198	17.10	33.2	121		s	805	238	19.29	7.7	367	4.4	b	987
199	19.00	6.0	125	4.1	b	815	239	19.00	47.5	1000		s	990
200	19.20	5.0	262	3.3	d	818	240	19.43	3.2	99	3.8	b	994

Table 1 (continued)

(1)	(2)	(3)	(4)	(5)	(6)	(7)	(1)	(2)	(3)	(4)	(5)	(6)	(7)
241	19.49	5.3	174		c	995	281	19.20	3.3	82	4.5	b	1130
242	16.46	2.1	9		s	999	282	18.30	19.8	219	5.8	d	1131
243	18.73	11.5	716		s	1001	283	18.10	15.6	143		s	1142
244	16.20	2.9	9	4.2	d	1002	284	18.02	5.1	125	4.1	b	1145
245	18.20	2.5	51		c	1003	285	18.89	7.7	147	5.5	b	1147
246	16.40	6.2	12	5.3	d	1004	286	18.90	4.6	182		c	1153
247	19.10	9.4	218		s	1005	287	18.00	19.8	340	6.2	d	1156
248	17.60	5.6	241	3.5	d	1006	288	18.70	28.7	459	6.3	d	1157
249	19.38	2.4	146	3.1	b	1010	289	18.80	5.4	94	3.5	d	1161
250	19.20	2.7	142	2.9	b	1011	290	17.50	6.6	26	3.1	d	1163
251	19.20	19.6	1014	5.7	d	1013	291	19.29	3.1	172		c	1166
252	18.40	3.1	77		c	1018	292	19.09	5.9	134		c	1176
253	17.90	25.0	191		s	1020	293	18.30	12.4	137	3.9	d	1177
254	18.80	2.8	49		c	1022	294	18.70	32.1	514	6.4	d	1179
255	17.70	28.0	178		s	1024	295	19.00	3.7	55	3.1	b	1194
256	16.60	17.5	37	5.5	d	1026	296	18.50	7.0	69	4.1	b	1203
257	19.30	5.1	291		c	1030	297	18.60	90.7	721	9.4	d	1211
258	19.30	9.0	245		zs	1031	298	19.00	5.5	115		c	1212
259	19.38	29.1	869	5.5	d	1035	299	19.50	14.9	1022	4.7	d	1215
260	18.50	4.1	54		c	1038	300	18.30	3.3	74		c	1216
261	19.47	18.7	608		s	1042	301	18.50	10.1	134	3.9	d	1219
262	19.50	5.0	339		c	1051	302	19.23	32.6	376	4.4	d	1222
263	18.44	2.8	71	3.3	b	1053	303	18.70	6.5	177	4.5	b	1228
264	18.50	2.4	31	4.3	b	1055	304	18.39	3.7	92		c	1242
265	16.40	7.9	15		s	1061	305	19.40	9.8	153		c	1248
266	19.40	3.8	240		c	1066	306	18.00	7.7	64	5.8	b	1249
267	18.10	2.2	20	3.4	b	1070	307	17.71	5.8	37	3.7	d	1254
268	18.00	3.1	53		c	1080	308	19.50	13.8	462	4.8	d	1263
269	19.10	30.3	335		s	1089	309	17.81	7.1	50	3.8	d	1265
270	18.50	6.8	73		zs	1090	310	18.60	2.4	35	3.7	b	1269
271	18.20	17.6	71		s	1097	311	18.70	14.5	232	4.4	d	1270
272	18.50	3.7	99		c	1101	312	19.40	5.2	159	3.3	b	1277
273	19.20	20.8	526	5.7	d	1102	313	19.10	108.6	5142	10.4	d	1278
274	19.20	4.1	66		c	1104	314	19.10	7.1	163	4.2	b	1281
275	19.50	9.7	290	4.7	b	1105	315	19.20	12.7	322		s	1288
276	18.80	7.8	211		s	1106	316	18.90	4.9	93	6.1	b	1299
277	19.10	2.3	53	3.2	b	1112	317	19.10	7.0	401	3.6	d	1300
278	18.20	3.0	30		c	1122	318	19.20	4.4	79	3.3	b	1304
279	19.40	4.9	150	3.5	b	1123	319	18.90	2.1	83		c	1309
280	18.50	3.0	37		zs	1129	320	16.90	10.6	723	4.0	d	1314

Table 1 (continued)

(1)	(2)	(3)	(4)	(5)	(6)	(7)	(1)	(2)	(3)	(4)	(5)	(6)	(7)
321	19.20	3.2	80		c	1319	361	17.70	4.8	31	5.4	b	1473
322	19.20	4.4	111		c	1326	362	17.70	9.1	119	4.9	b	1474
323	17.50	6.2	384	4.0	b	1327	363	19.00	3.2	139		c	1475
324	18.80	2.6	34	3.3	b	1328	364	18.80	4.5	53		c	1480
325	18.40	4.7	56	4.8	b	1331	365	18.50	9.2	119	4.3	d	1487
326	18.71	3.5	45	3.3	d	1334	366	18.93	3.4	49	3.3	b	1504
327	18.80	3.6	62		c	1339	367	19.40	4.3	268		c	1507
328	17.64	6.7	291	3.8	d	1356	368	19.10	64.2	498		zs	1508
329	18.50	8.2	354	4.1	d	1358	369	19.40	4.5	79	4.7	b	1512
330	19.30	35.2	407	4.5	d	1363	370	17.80	7.4	290		s	1523
331	19.07	28.3	1302	5.4	d	1368	371	17.60	5.8	83	3.8	d	1524
332	19.00	35.8	754	6.8	d	1381	372	18.10	2.7	51		c	1527
333	18.90	3.3	63	5.7	b	1383	373	18.70	3.1	49		c	1528
334	18.60	6.7	59	3.9	d	1386	374	19.10	14.5	81		s	1533
335	18.90	3.7	145	3.9	b	1389	375	19.30	5.8	108		s	1536
336	19.20	3.8	96	3.2	b	1393	376	19.30	151.1	4201	9.2	d	1539
337	19.20	2.5	131		c	1396	377	19.00	2.8	120	2.9	b	1541
338	19.00	38.6	813	10.7	b	1400	378	18.80	5.8	101	5.2	b	1543
339	18.70	84.1	2752	9.1	d	1402	379	18.80	46.8	369	4.2	d	1547
340	17.50	7.1	28	3.2	d	1404	380	19.00	5.2	75	4.5	b	1548
341	19.40	100.6	3068	9.9	d	1405	381	18.50	9.3	124	4.2	d	1551
342	18.61	118.6	1746	10.2	d	1406	382	18.10	8.5	57	2.9	d	1553
343	19.41	2.4	73	4.2	b	1408	383	18.99	5.7	118	4.6	b	1556
344	17.20	11.9	41		s	1413	384	19.40	4.1	255	3.3	b	1560
345	18.10	3.9	73	3.4	d	1414	385	19.00	3.3	50	2.5	b	1561
346	18.70	3.5	55		c	1422	386	19.30	2.9	58	3.6	b	1567
347	18.90	7.9	152	4.6	b	1426	387	19.27	9.2	158		c	1568
348	17.90	3.5	20		c	1427	388	19.42	3.4	75	2.7	b	1569
349	18.09	7.5	68	4.5	d	1431	389	18.00	2.8	48	3.0	d	1571
350	18.65	4.3	133		c	1434	390	17.40	8.7	341	4.3	d	1573
351	19.40	2.5	53	2.9	b	1436	391	16.60	27.0	127	5.5	d	1575
352	19.00	2.1	91		c	1440	392	19.00	2.7	114	3.6	b	1576
353	18.60	2.0	29	3.4	b	1448	393	18.00	63.8	282		s	1579
354	18.40	2.2	55		c	1451	394	16.48	44.5	66	4.7	d	1588
355	18.40	5.6	67	4.4	b	1453	395	19.50	4.6	68	3.6	b	1589
356	18.99	5.3	100	3.5	d	1460	396	18.10	3.4	23		c	1607
357	18.40	3.5	23		zs	1463	397	19.30	5.0	284		s	1613
358	18.80	2.2	80		c	1465	398	18.31	2.6	22		c	1617
359	18.50	4.1	111	3.1	d	1466	399	18.79	4.0	50	2.9	b	1625
360	17.95	5.5	258		s	1467	400	19.10	2.6	44	2.5	b	1630

Table 1 (continued)

(1)	(2)	(3)	(4)	(5)	(6)	(7)	(1)	(2)	(3)	(4)	(5)	(6)	(7)
401	19.30	13.9	223		s	1637	441	18.40	23.1	280		s	1779
402	17.10	3.0	23	3.8	d	1644	442	18.82	204.7	3658		zs	1780
403	18.50	3.1	84	3.9	b	1648	443	19.30	4.3	83		c	1781
404	19.30	6.5	275	4.1	b	1650	444	19.20	29.6	751	6.5	d	1783
405	18.20	9.6	69	3.6	d	1660	445	19.01	59.9	2608	7.6	d	1790
406	19.37	4.4	90	3.7	b	1661	446	19.00	2.8	43		c	1793
407	19.38	21.3	1303	6.2	d	1665	447	18.86	2.2	40	4.5	b	1794
408	19.11	7.8	441	4.7	b	1667	448	18.40	8.3	71	3.0	d	1796
409	19.50	2.8	92	2.9	b	1670	449	19.00	88.8	548	6.5	d	1800
410	18.90	5.4	73		c	1671	450	18.11	8.6	58	3.0	d	1805
411	19.01	3.4	52	3.3	b	1677	451	19.19	5.6	97	3.7	b	1808
412	19.20	4.6	82		c	1685	452	18.70	32.1	513	6.4	d	1810
413	19.16	5.0	85	3.3	b	1686	453	19.10	3.2	54	2.7	b	1811
414	19.20	4.6	81	2.5	b	1700	454	19.40	50.7	3163	7.5	d	1813
415	18.40	8.2	56	5.4	b	1701	455	18.90	23.3	249		s	1818
416	18.51	2.3	23	3.9	b	1704	456	18.64	5.0	54	2.9	b	1820
417	19.20	3.5	182	3.7	b	1707	457	18.80	2.8	102	3.2	b	1821
418	18.90	29.8	295	3.9	d	1708	458	17.08	13.7	100		s	1825
419	19.00	36.7	356	4.9	d	1714	459	19.20	6.6	113	4.6	b	1829
420	18.90	4.6	115	3.8	b	1720	460	19.30	5.8	108		c	1838
421	19.10	16.8	224		s	1728	461	19.40	122.5	674	7.7	d	1840
422	18.10	16.1	68		s	1731	462	19.30	5.6	105	2.9	b	1852
423	16.70	10.6	27	5.0	d	1733	463	18.85	21.9	230		s	1855
424	19.18	4.7	81	3.8	b	1734	464	18.90	3.4	135		c	1866
425	16.40	427.1	369		zs	1735	465	18.50	13.1	117	3.8	d	1867
426	19.50	2.5	83		c	1736	466	19.35	6.0	118	3.1	b	1870
427	18.20	4.1	30	2.9	b	1737	467	19.10	4.5	73	3.2	b	1875
428	18.40	2.6	24	3.1	b	1741	468	19.10	2.2	103		c	1878
429	18.70	4.2	49		c	1747	469	18.34	7.7	63		c	1895
430	19.30	8.3	148	4.6	b	1749	470	19.20	2.7	50	3.5	b	1897
431	19.10	61.3	488		s	1750	471	18.10	3.4	63	3.6	b	1900
432	16.40	27.4	39		s	1751	472	19.00	6.6	96	4.1	b	1904
433	19.10	33.2	355		s	1761	473	19.48	3.0	69	3.4	b	1909
434	19.30	2.7	55	2.6	b	1764	474	18.66	46.2	339	5.1	d	1913
435	19.40	6.6	199		c	1765	475	18.96	11.5	149	3.3	d	1914
436	18.20	10.2	73	4.5	b	1766	476	19.40	127.9	681	6.7	d	1915
437	19.26	2.7	145		c	1770	477	18.80	2.3	31	2.4	b	1922
438	18.26	2.0	44		c	1775	478	18.80	2.3	30	2.8	b	1923
439	16.49	44.9	67	4.9	d	1776	479	19.00	8.2	116	2.7	d	1925
440	19.38	3.4	73	4.4	b	1777	480	19.19	4.2	74	3.0	b	1930

Table 1 (continued)

(1)	(2)	(3)	(4)	(5)	(6)	(7)	(1)	(2)	(3)	(4)	(5)	(6)	(7)
481	19.44	13.9	245		s	1931	521	19.40	2.1	48		c	385
482	18.90	3.1	43		c	1939	522	18.91	6.0	116		c	535
483	19.40	6.1	124		c	1942	523	19.30	6.7	187	4.2	b	638
484	19.30	2.6	53	2.8	b	1943	524	19.00	2.5	53		c	659
485	19.20	4.7	83	3.3	b	1946	525	19.20	2.2	139		c	669
486	19.18	9.5	152	3.8	b	1954	526	19.15	83.7	2026		s	688
487	18.80	38.4	328		s	1964	527	18.70	4.7	75		c	781
488	18.57	6.2	63	2.8	d	1973	528	18.90	7.0	228		s	809
489	19.24	12.2	194	3.9	b	1974	529	18.60	4.2	61		c	836
490	19.24	1.9	37		c	1976	530	19.18	30.3	1542	5.0	d	911
491	18.00	9.9	60	3.9	b	1979	531	17.70	6.6	42	3.8	d	920
492	19.40	10.0	186	4.8	b	1987	532	19.40	5.3	328		s	1090
493	18.74	5.4	64	3.3	b	1990	533	19.50	20.7	693		c	1127
494	18.37	5.1	44	3.9	b	1991	534	18.20	18.1	72	4.9	d	1270
495	17.42	4.8	18		s	1992	535	17.00	2.8	9	3.7	d	1273
496	19.24	10.8	176	4.3	b	2002	536	19.18	3.1	77		c	1285
497	19.47	3.7	84	2.7	b	2003	537	18.40	16.8	204	6.4	b	1294
498	16.10	3.5	4	3.8	d	2022	538	18.40	35.9	436	5.6	d	1332
499	19.00	3.0	46	2.3	b	2025	539	18.80	5.0	178		s	1517
500	18.95	11.3	146		s	2031	540	17.89	3.7	57	3.5	d	1591
501	18.90	22.9	246	4.8	b	2043	541	19.00	5.7	295	4.1	b	1624
502	19.10	3.1	51	2.5	b	2059	542	18.60	4.0	118		c	1647
503	18.10	2.6	18		c	2067	543	18.70	3.8	122		c	1662
504	19.44	4.4	96		c	2068	544	18.80	22.5	394		s	1763
505	19.00	8.6	121		c	2075	545	17.76	2.1	29	3.3	b	1879
506	18.70	31.5	270	5.3	b	2077	546	17.20	17.4	142		s	1880
507	19.30	49.8	483		s	2085	547	18.70	6.5	146		s	1908
508	17.90	5.3	31	3.6	b	2086	548	19.30	119.7	656	7.2	d	2004
509	19.23	28.5	348		s	2087	549	18.04	21.3	123		s	2143
510	18.62	13.6	132		s	2091							
511	18.10	2.9	20	4.1	b	2102							
512	17.94	33.5	167		s	2103							
513	18.00	6.6	41	2.8	d	2107							
514	18.40	7.4	64		c	2117							
515	17.85	3.1	17	3.3	b	10							
516	18.30	138.4	505	6.5	d	60							
517	17.20	76.7	187		s	104							
518	19.10	2.1	36	2.9	b	266							
519	17.89	8.1	45	4.6	b	286							
520	18.83	2.9	52	3.6	b	349							

1 — sizes are presented only for objects of b and d types,
2 — at the end of this column the numbers are given from the unpublished version of the catalogue (Ivanov et al., 1993).